Aerosol and Air Quality Research, 14: 559–571, 2014

ISSN: 1680-8584 print / 2071-1409 online
doi: 10.4209/aaqr.2013.06.0198

Overview of Chemical-Looping Reduction in Fixed Bed and Fluidized Bed Reactors Focused on Oxygen Carrier Utilization and Reactor Efficiency

Zhiquan Zhou, Lu Han, George M. Bollas*

Department of Chemical & Biomolecular Engineering, University of Connecticut, Storrs, Connecticut, USA

ABSTRACT

A model-assisted comparison of two types of chemical-looping (CL) reactors (fixed bed and fluidized bed), with the same oxygen carrier loading and fuel capacity, is carried out to examine performance and efficiency of CL Reducers, operating with methane as the feedstock and nickel oxide as the oxygen carrier. The study focuses on the reduction step of chemical-looping combustion (CLC), for which the reactor efficiency and fuel utilization are crucial in terms of economics and carbon capture efficiency. Process models (a three phase dynamic model for bubbling fluidized beds and a two dimensional homogeneous model for fixed beds) and reaction kinetics developed and validated in previous studies are used. A fluidized bed chemical-looping combustion Reducer is compared to a fixed bed equivalent reactor, scaled-up from a smaller experimental reactor, constrained to bed height to reactor diameter ratios that prohibit excessive temperature and pressure drops across the bed. Through a detailed comparison, CLC operated in the fluidized bed reactor is shown to deliver superior performance, i.e., uniform temperature and pressure distribution; high methane conversion (> 95%) and carbon dioxide selectivity (> 95%) sustained for longer reduction periods; negligible carbon formation (< 2 mol% C basis); and better efficiency in oxygen carrier utilization.

Keywords: Fixed bed; Fluidized bed; Chemical-looping combustion; Reactor scale-up.

INTRODUCTION

Significant progress has been made towards a better understanding of the risk factors to climate change in the last decade; the accumulation of greenhouse gas from combustion of fossil fuels in the power and transportation sectors has been confirmed as the main contributor to climate change (IEA, 2011). CO_2 is the leading anthropogenic greenhouse gas and is projected to increase globally in the near future due to fossil fuel use and land use change (Solomon *et al*., 2007). An effective solution to reduce CO_2 emissions from existing fossil fuels-based power plants is to implement CO_2 capture and sequestration technologies. Currently, the main approaches to CO_2 capture for industrial power plants (pre-combustion, post-combustion, and oxy-fuel combustion) are energy intensive (Toftegaard *et al*., 2010) and great research effort has been put to develop new low-cost technologies. Chemical-looping combustion (CLC) has emerged as a novel process for power production using fossil fuels with low cost and efficient CO_2 separation. The basic concept of the process involves two interconnected reactors, a Reducer and an Oxidizer, with an oxygen carrier (OC) - a metal/metal oxide - circulating between the two reactors. The principle of CLC (Fig. 1) is based on enabling hydrocarbon combustion in the absence of N_2, which accomplishes fuel oxidation with in-situ CO_2 separation (CO_2 is separated by condensing the water vapor in the effluent of the Reducer). Different metal oxides have been proposed and tested as promising candidates, including CuO, NiO, Fe_2O_3, and Mn_2O_3 (Mattisson *et al*., 2004). The development and testing of oxygen carriers in lab- and bench-scale reactors have been heavily studied, with more than 700 carriers already tested (Adánez *et al*., 2012). A number of oxygen carriers were proven to demonstrate satisfactory performance with respect to fuel and oxygen carrier conversion and stability over continuous operation. Ni-based oxygen carriers are the most extensively analyzed materials in the literature due to their high reactivity towards combustion of CH_4 and high melting point, which allows for higher operating temperatures (Mattisson *et al.*, 2006; Sedor *et al.*, 2008). The reduced Ni is also a catalyst for many reforming reactions, however depending on the availability of oxygen, carbon deposition on the surface may occur. This is undesired, because carbon will be oxidized in air, undermining the carbon capture efficiency of the system. Other disadvantages of Ni-based oxygen carriers include their high cost and toxicity (Adánez *et al.*, 2012); while Cu and Fe-based oxygen carriers are less expensive and more

* Corresponding author.
Tel.: + 860 486 4602
E-mail address: george.bollas@uconn.edu

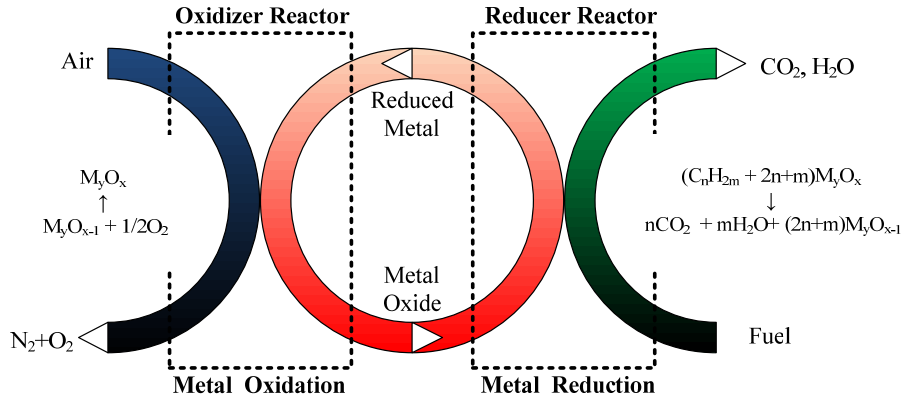

Fig. 1. Basic concept of chemical-looping combustion process.

environmentally benign. High reaction rates are expected for Cu-based OCs. However, Cu-based OCs exhibit agglomeration and sintering as a result of the low melting point of Cu. Because of the low oxygen capacity of Fe-based oxygen carriers, higher active Fe_2O_3 content is preferred (> 60 wt%). Overall, material handling and oxygen carrier selection are critical to the future of industrial-scale application of CLC technology (Rubin *et al.*, 2012).

Different reactor concepts have been implemented for testing suitable oxygen carriers for CLC, including alternating fixed bed reactors (Noorman *et al.*, 2007), interconnected fluidized bed reactors (Pröll *et al.*, 2009) and rotating reactors (Håkonsen and Blom, 2011). Early experimental studies on CLC were conducted in thermogravimetric analyzers (TGA) and fixed bed reactors. Both are commonly used for kinetic studies because of their simplicity, favoring reaction rates to be extracted easily from experimental data (Abad *et al.*, 2007; Iliuta *et al.*, 2010; Jin and Ishida, 2002). These systems however, implement semi-batch processes and as a result flow rates must be switched periodically. For industrial application, chemical-looping is conceptualized as a dual fluidized bed technology (Lyngfelt *et al.*, 2001; Adánez *et al.*, 2006; Pröll *et al.*, 2009; Sridhar *et al.*, 2012), where particles are continuously transported between the Reducer and Oxidizer.

A main drawback of the fluidized reactor concept is associated with attrition of the solids due to the mechanical and chemical stress (enhanced by the redox conditions of CLC) in a fluidized environment. Generation of fines (particles smaller than 45 μm) may lead to gradual degradation of bed particles (Lyngfelt and Thunman, 2005) that can be entrained out of the system and necessitate larger separation and collection systems and replacement of the lost solids. The standard ASTM attrition test (ASTM, 1995) at relevant CLC industrial operation was used to determine the long-term attrition behavior of different oxygen carriers (Baek *et al.*, 2010, 2011). Kramp *et al.* (2011) used attrition models to simulate large-scale interconnected fluidized bed reactor, based on small/pilot-scale experimental investigations of the attrition behavior and quantified the oxygen carrier loss that results from attrition and inefficient solids separation. Their simulation results show that most of the attrition is mainly generated in the cyclones, and accounts for a loss of 2.05 kg/MWh at the pilot scale and 2.25 kg/MWh in a 100 MW_{th} unit. On the contrary, the solids inside the fixed bed reactor are stationary, and thus attrition issues are intrinsically avoided (Solunke and Veser, 2010). To process large inventories of solids, pressure drop and temperature control are important factors that also influence the performance of large fixed beds. Regarding the design of oxygen carriers, larger sizes are favored for fixed bed reactors to minimize pressure drop and plugging, whereas fluidized beds are capable of using smaller particles with the minimum fluidization condition being easily satisfied (Kunii and Levenspiel, 1968a, b). Particle agglomeration is another issue which cannot be ignored for CLC systems with two interconnected fluidized beds, especially with Cu-based oxygen carriers. Agglomeration can cause bed defluidization, leading to solid circulation disturbance, gas channeling and less gas-solid contact. In fixed beds, loss of available surface area due to agglomeration can cause severe decrease in oxygen carrier performance over time.

In the open literature, authors have primarily focused on either fixed bed or fluidized bed reactors and few comparable results are available. It is the intention of this work to compare the performance (primarily, the oxygen carrier utilization and reactor efficiency) of fixed bed and fluidized bed reactors, in which the same oxygen carrier, solid loading and fuel flow are utilized. An emphasis is placed on the scalability of a fixed bed reactor to match the capacity of an existing CLC fluidized bed unit. Within the CLC community, limited CLC larger-scale plants have been developed (Ryu *et al.*, 2004; Lyngfelt and Thunman, 2005; Adánez *et al.*, 2006; Kolbitsch *et al.*, 2009; Mattisson *et al.*, 2009; Wang *et al.*, 2010; Rifflart *et al.*, 2011), and there is less emphasis on the scalability to large-scale reactors. Nevertheless, scale-up of CLC reactor systems is of high significance in CLC technology.

In this work, Ni-based kinetics network and parameters validated in previous studies (Zhou *et al.*, 2013, 2014; Han *et al.*, 2013) and transient non-ideal reactor models developed for two types of Reducers: fixed and fluidized beds are used to predict the performance of CLC reduction. Based on the developed reactor model, scale-up of the fixed bed reactor is performed to meet design criteria that make it comparable to its fluidized bed equivalent. Real

CLC performance metrics based on carbon formation, oxygen carrier conversion, fuel conversion, and CO_2 selectivity are shown for each reactor. Spatial and transient pressure and temperature variations are shown and analyzed. Other issues, like challenges in operating CLC at minimum oxygen carrier loading (therefore, smaller Reducer size), OC loading required for high CH_4 conversion and OC conversion, time required for significant carbon formation at a given OC loading, and CO_2 selectivity of fluidized bed and scale-up fixed bed units are discussed. It is assumed that a successfully operated semi-batch fluidized bed CLC Reducer (in terms of conversion and CO_2 selectivity) would translate into successful operation at steady state (integrated with the Oxidizer in a real CLC pilot plant). However, the implications of converting semi-batch performance to steady state performance are not within the scope of this work.

MODEL DESCRIPTION

The objective of this study is to investigate the performance and efficiency of two types of reactors in implementation of CLC. In each reactor system, the reduction of a NiO-oxygen carrier with methane feedstock is explored. A semi-batch fluidized bed unit from the literature (Chandel *et al.*, 2009) is chosen as the prototype reactor in this analysis. A fixed bed reactor is designed, based on the experimental setup of Iliuta *et al*. (2010) to match the feed flow and solids inventory of the fluidized bed reactor. Both prototype reactors are assumed to process preheated, undiluted methane and to not be externally heated, which are realistic conditions for an industrial-scale application. Table 1 summarizes the geometries and operation of the fluidized bed and scaled-up fixed bed reactor units. The typical initial temperature for a steady-state CLC Reducer is 900°C (Adánez *et al.*, 2009).

Reaction Kinetic Network

Table 2 shows the reaction scheme used in this study for a Ni-based, CH_4-fed CLC system. The reaction scheme and kinetics have been validated against published fixed bed chemical-looping units from the literature (Ryu *et al*., 2003; Corbella *et al*., 2005, Rydén *et al*., 2008; Iliuta *et al*., 2010) and in-house fixed bed experiments (Zhou *et al.*, 2013); and were further validated against reported fluidized bed experimental data from the literature (Chandel *et al.*, 2009; Ryu *et al.*, 2009; Iliuta *et al*., 2010) with a three-phase fluidized bed model (Zhou *et al.*, 2014). Reactions involved include NiO reduction reactions (with CH_4, H_2 and CO), Ni-catalyzed reforming reactions (steam reforming, dry reforming and water gas shift reaction) and Ni-catalyzed carbon formation or elimination reactions (CH_4 decomposition and carbon gasification by H_2O and CO_2). The kinetic expressions, kinetic parameters, thermodynamic equilibrium constants, and adsorption coefficients for all the reactions studied were shown and discussed in detail in previous work (Zhou *et al.*, 2013).

Fluidized Bed Model

A dynamic three-phase (bubble, emulsion and wake) flow model is used to predict bubbling bed hydrodynamics (Kunii and Levenspiel, 1968a, b) in the semi-batch reactor of Chandel *et al.* (2009). The model considers gas bubbles flowing through a dense emulsion phase at a relative

Table 1. Geometries and operating conditions of the fixed bed and fluidized bed units.

Properties	Fluidized bed unit	Fixed bed unit
Inlet temperature(°C)	900	900
NiO/support	60% $NiO/NiAl_2O_4$	60% $NiO/NiAl_2O_4$
OC load (kg)	2.5	2.5
Particle size (μm)	171	171
CH_4 composition	100%	100%
Gas flow rate (m^3/s)	0.000278	0.000278
I.D. (mm)	96	60
Bed height (m)	0.15	0.223
L/D	1.56	3.717
Bed porosity	0.65–0.7	0.37
Bulk density (kg/m^3)	2200	3960

Table 2. CH_4-NiO chemical-looping reaction network.

Oxygen carrier reduction reactions	Partial CH_4 oxidation	$CH_4 + 2NiO \leftrightarrow 2Ni + CO_2 + 2H_2$	(R1)
	H_2 oxidation	$H_2 + NiO \leftrightarrow Ni + H_2O$	(R2)
	CO oxidation	$CO + NiO \leftrightarrow Ni + CO_2$	(R3)
	Partial CH_4 oxidation	$CH_4 + NiO \leftrightarrow Ni + 2H_2 + CO$	(R4)
Reactions catalyzed by Ni	Steam reforming	$CH_4 + H_2O \leftrightarrow 3H_2 + CO$	(R5)
	Water gas shift	$CO + H_2O \leftrightarrow H_2 + CO_2$	(R6)
	Dry reforming	$CH_4 + CO_2 \leftrightarrow 2CO + 2H_2$	(R7)
	Methane decomposition	$CH_4 \leftrightarrow 2H_2 + C$	(R8)
	Carbon gasification by steam	$C + H_2O \leftrightarrow CO + H_2$	(R9)
	Carbon gasification by CO_2	$C + CO_2 \leftrightarrow 2CO$	(R10)

velocity given by the minimum fluidization velocity, with gas percolating through the bed of solids. Rising bubbles are accompanied by a wake of solids and this is the main mechanism causing solids circulation (Fig. 2). A small fraction of the solids that reach the dense bed top is entrained in the freeboard, whereas the rest of the solids flow downwards, forming countercurrent flow and establishing good mixing between gas and solids in the emulsion phase.

The diameter of bubbles increases with bed height, but is the same over the cross section of the bed at any bed height. As shown in Fig. 2, gas/solid exchange between the bubble/wake and emulsion phases is taken into account via mass diffusive and convective transfer. Two temperature profiles (bubble/wake and emulsion) are calculated for the dense phase, assuming the same temperature for the gas and solids in each phase. The temperature difference between the two phases is determined by interphase heat transfer and reaction heat generation or consumption. Entrainment of particles from the bed into the freeboard is considered; while elutriation of solids out of the freeboard is neglected. The freeboard region is modeled as a one-dimensional two-phase (gas and solid) transient plug flow reactor. The basic differential equations of the model are given in the Appendix. Detailed equations and the application of this model on various bubbling fluidized bed CLC experimental data of the open literature are presented in Zhou *et al*. (2014). The model performance and accuracy, as applied on the data by Chandel *et al.* (2009) are shown in Fig. 3(b). The validity of the bubbling bed regime hypothesis for this data is articulated in the following.

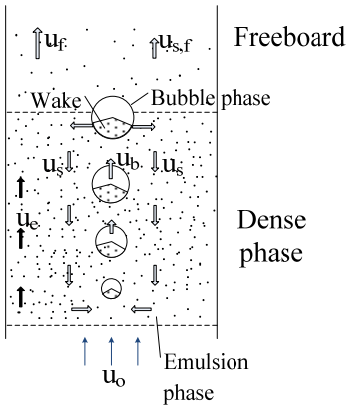

Fig. 2. Bubbling fluidized bed reactor physical model.

Fig. 4 shows a representation of various fluidization regimes for Geldart type A and B particles, by defining the dimensionless particle size, $d_P^* = Ar^{1/3}$, and the dimensionless velocity, $U^* = Re/Ar^{1/3}$, where Ar is the Archimedes number and Re is the Reynolds number. The analysis is based on the work of Bi and Grace (1995) updated to account for the newer and more general correlation of Haider and Levenspiel (1989) for the particle terminal velocity, U_t^*, and the recent correlation of Olazar *et al.* (2009) for the minimum spouting velocity, U_{ms}^*, in conical spouted beds at high temperatures. The shaded areas in Fig. 4 illustrate ranges of stable operation in the corresponding hydrodynamic regime (Bubbling Fluidization, Fast Fluidization, Conveying (Yang, 2003), and Spouting in conical reactors (Olazar *et al.*, 2004)). U_c^* and U_{se}^* depict the theoretical upper bound of stable stagnant fluidization and the critical velocity of entrainment, respectively. Bubbles appear at the minimum fluidization velocity for Gerdart B particles and are distinct up to turbulent fluidization, when superficial velocity becomes more vigorous (Re_c in Fig. 4). The operation of self-sustained fluidized beds is terminated when significant entrainment of particles occurs (Re_{ce} in Fig. 4). Depending on the bed position and reaction time (affecting temperature and gas composition), a range of d_P^* and U^* for the unit of Chandel *et al.* (2009) was obtained (dots in Fig. 4, enclosed within the dark shaded area), which falls into the bubbling fluidization regime. According to the Yagi and Muchi correlation, slugging is unlikely to occur for this unit ($H_{bed} = 0.15 < D_R/(\rho_s d_P)^{0.3} = 0.18$) (Rhodes, 2008).

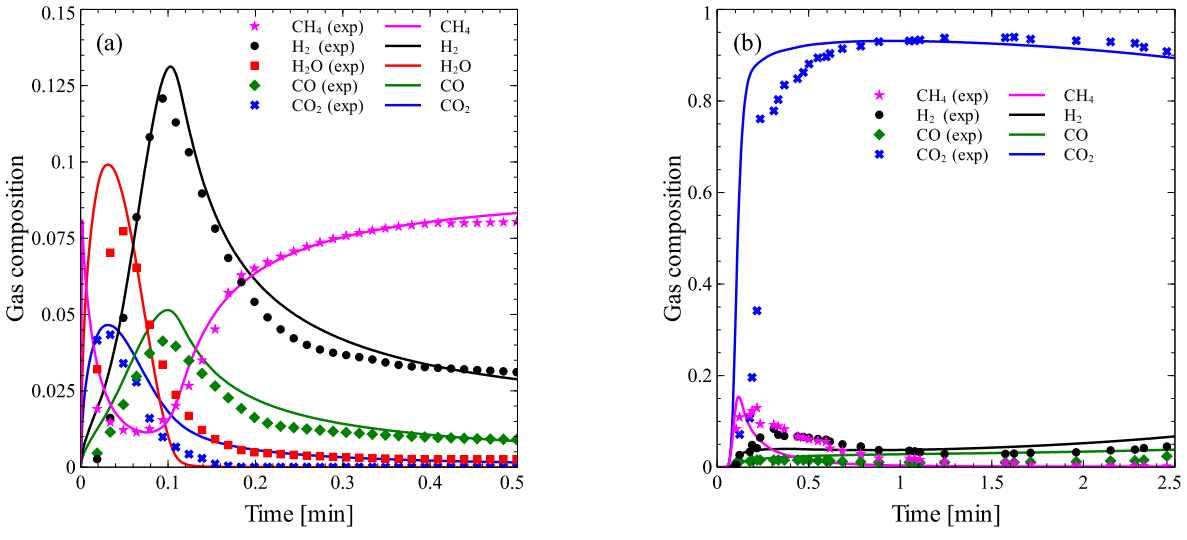

Fig. 3. Chemical-looping reduction selectivity using Ni/NiO and CH_4 in a fixed bed reactor and a bubbling bed reactor: experimental data from: (a) Iliuta *et al*. (2010) at 900°C and (b) Chandel *et al*. (2009) at 800°C.

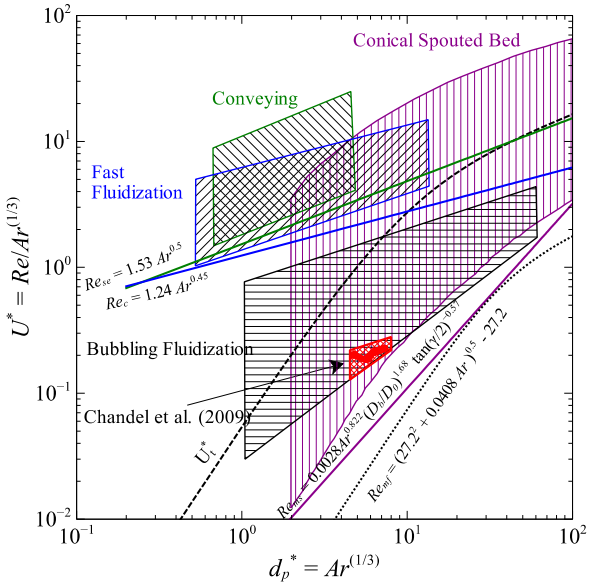

Fig. 4. Regimes of gas – solid fluidization (Bi and Grace, 1995) and validity of the bubbling bed regime hypothesis for the data published by Chandel *et al*. (2009).

The average particle diameter used in Chandel *et al.* (2009) is 171 μm and, therefore, intraparticle diffusion is neglected in this study. This is due to the fact that diffusion limitations on reaction rates are not significant for small oxygen carriers (< 200 μm) (García-Labiano *et al.*, 2005; Han *et al.*, 2013). Previous work (Han *et al.*, 2013) showed that the effectiveness factors for the non-catalytic and catalytic reactions remain close to unity during chemical-looping reduction using a particle of 140 μm in diameter. The reactor regime can be approximated as homogeneous up to mean particle diameters of 800 μm, at which point intraparticle diffusion begins to lower the reaction rates (Han *et al.*, 2013).

Fixed Bed Model

The governing equations consider mass and heat transport in the axial and radial direction of the fixed bed. The transport mechanism is considered to be a transient, axially and radially dispersed plug flow. Variations in the radial direction of the column are necessary to model, because cold spots from the endothermic reactions can affect conversion and selectivity of the oxygen carrier and impact the overall design of the reactor. Effective transport correlations from experimental studies are used to cover a wide range of flow conditions. Pressure drop across the bed is accounted for by the Ergun equation, which satisfies laminar and turbulent flow regimes. The two-dimensional homogeneous model is chosen for this system because intraparticle gradients are negligible within the small particles studied here (Han *et al.*, 2013). The fixed bed model has been successfully used to predict the fixed bed CLC experimental results published by Iliuta *et al.* (2010) (Fig. 3(a)). The reactor utilized by Iliuta *et al*. (2010) is micro-scale in nature, and a scale-up step is required to arrive at a size to be compared with the fluidized by Chandel *et al.* (2009), which is used as the base-case in this analysis.

Scale-up of Fixed Bed Reactor

The scale-up of the fixed bed reactor is achieved by increasing the length and diameter of a single tube. As previously mentioned, the oxygen carrier loading and fuel flow rate are set equal to those of the fluidized bed reactor. Among the several ways to increase the capacity of a fixed bed reactor, the strategy used here maintains geometric similarity (length to diameter ratio of the fixed bed) to the small-scale reactor (Nauman, 2008). As the flow regime is laminar in both cases, scaling with geometric similarity is often adhered to. The L/D ratio for the micro-reactor used by (Iliuta *et al.*, 2010) is 1.9, and when implemented in large-scale fixed bed, temperature variations present an issue. Iliuta *et al.* (2010) approximated their micro-reactor as isothermal because the reactor was placed inside a furnace and the fuel was diluted in 90% Ar, which limited heat consumption due to endothermic reduction and reforming reactions. However in the large-scale reactor, external heating and fuel dilution cannot be maintained due to cost considerations. This leads to challenges in maintaining high fuel conversion as well has high CO_2 selectivity. The geometry of the scaled-up fixed bed reactor was initially chosen (D = 7.5 cm; L = 14.3 cm) to maintain the same L/D ratio as the micro fixed bed reactor used by Iliuta *et al.* (2010). Simulations performed with this reactor geometry exhibit poor fuel conversion caused by severe temperature fluctuations across the fixed bed. As a result, an additional step is needed to determine an optimal geometry for the reactor to achieve the desired conversion level (Kim *et al.*, 2012). In this work, optimal geometry of the reactor is determined by carrying out simulations of the model for a range of L/D ratios from 1.9 to 5.0, incrementing by 0.1. The selection criteria are the following: temperature drop < 250°C, 99% CH_4 conversion for over 200 seconds, and pressure drop < 1 bar. It was observed that a L/D ratio of 3.8 fulfills these criteria, is still within the range of many fixed bed chemical-looping reactors, and is realistic for practical commercial operation. After several iterations, the optimal L/D ratio to conduct CLC in fixed bed is found to be double that of the microreactor of Iliuta *et al.* (2010). The optimal geometry of the prototype fixed bed reactor is listed in Table 1.

RESULTS AND DISCUSSION

NiO Conversion Evolution over Time

In CLC reduction, the conversion of NiO follows different profiles due to the dynamics associated with each reactor. Fig. 5(a) shows the average NiO conversion in a fixed bed reactor, where 95% of the conversion is met within 6 minutes. In comparison, the fluidized bed reactor achieves 95% conversion in 3 minutes (Fig. 5(b)). The difference in time scale between the two reactors is attributed in part to longer contact times in the fluidized bed reactor. Higher reaction times of the gas inside the reactor lead to faster conversions of the oxygen carrier. Also, temperature drop is less severe in the fluidized bed because of the favorable

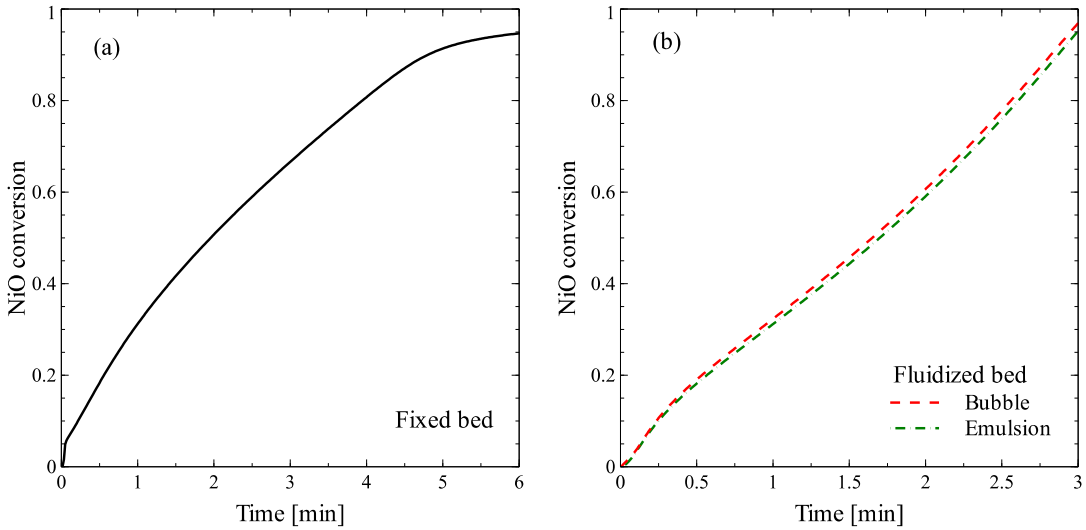

Fig. 5. Prediction of transient profiles of the degree of reduction of chemical-looping oxygen carrier using Ni/NiO and CH_4 in (a) fixed bed reactor and (b) bubbling bed reactor.

gas-solid mixing. Because of the endothermic nature of CLC, lower temperatures negatively affect the reaction rates and lower the conversion rate for the fixed bed reactor. The temperature profiles for the fluidized bed and fixed bed reactors are discussed in more detail in a following section.

Carbon Formation with Respect to NiO Conversion and Time

Carbon formation increases with time and NiO conversion. The CLC process should be run with complete or very high fuel conversion; the amount of available oxygen in the oxygen carrier should be well over the point where carbon deposition is favorable (e.g., oxygen supply to CH_4 ratio should be > 4 (Jerndal *et al.*, 2006)). However, since both reactors in this study are semi-batch type units, the excessive amount of NiO cannot be always guaranteed for the duration of the reactions; thus, carbon formation has to be considered where the local or total oxygen supply becomes insufficient. Figs. 6 and 7 show the total carbon formation w.r.t to NiO conversion and reduction time. In the initial 30 s for both reactors, no carbon is produced because of the large amount of NiO present. Carbon deposition appears more dominant at the end of the reduction phase when most of the NiO is consumed. Nearly 10 mol% carbon (CH_4 basis) is deposited in 6 minutes when 90% NiO conversion is achieved in the fixed bed reactor; whereas significantly smaller amount of carbon is formed in the bubbling fluidized bed at the same solid conversion. This can be explained by the fact that in the fixed bed reactor, NiO at the entrance of the reactor is immediately reduced to metallic Ni, creating a catalytic surface that initiates reforming and carbon formation reactions. The catalytic zone expands to the majority of the bed length at the end of reduction time. This should be compared with conditions in the fluidized bed, where the bed (mostly the emulsion phase) is well mixed. The rapid mixing and movement of solids allow efficient gas-solid contacting; therefore, CH_4 co-exists with the available NiO instead of catalytic Ni. An almost double

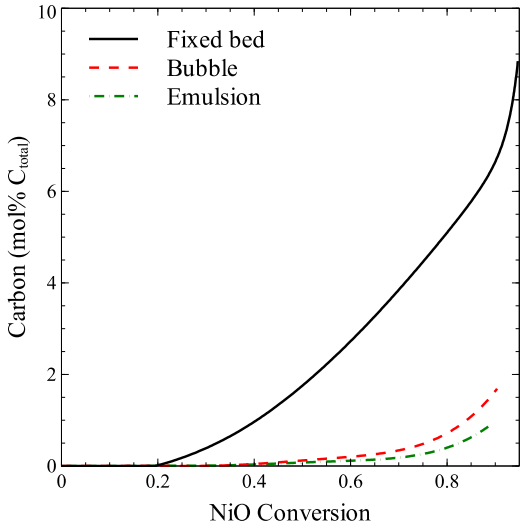

Fig. 6. Prediction of chemical-looping carbon formation with respect to the degree of reduction of oxygen carrier using Ni/NiO and CH_4 in fixed bed and bubbling bed reactors.

amount of carbon is generated in the bubble phase than in the emulsion phase; and this can be explained by the excess of oxygen carrier in the emulsion phase (~5% in bubble and ~95% in emulsion) and the relatively low mass transfer between the solids phases (emulsion and wake). The higher availability of oxygen source in the emulsion phase allows for lower carbon formation.

CO_2 Selectivity

One of the main benefits of the CLC process is the inherent CO_2 separation; thus a good CLC reactor design should be able to maintain high CO_2, and low CO and CH_4 concentrations for the entire reduction period. The CO_2 selectivity in the two types of reactors is presented in Fig. 8. In the fixed bed reactor, CO_2 selectivity varies considerably with solid conversion where upon initiation of CLC,

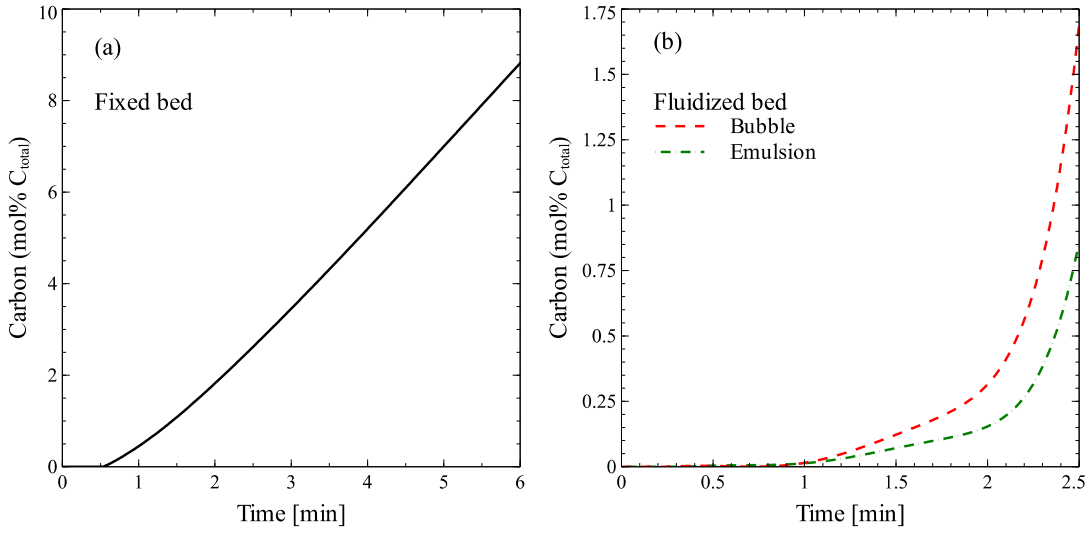

Fig. 7. Prediction of transient profiles of chemical-looping carbon formation using Ni/NiO and CH_4 in (a) fixed bed reactor and (b) bubbling bed reactor.

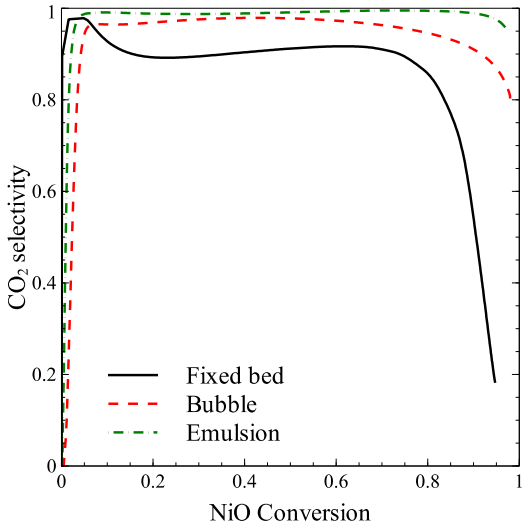

Fig. 8. Prediction of chemical-looping CO_2 selectivity with respect to the degree of reduction of oxygen carrier using Ni/NiO and CH_4 in fixed bed and bubbling bed reactors.

selectivity quickly increases to 0.96 before NiO conversion reaches 20%, drops to 0.9 when the NiO conversion is around 80% and further decreases to 0.2 when NiO conversion approaches unity. The observation that the CO_2 selectivity drops as NiO is gradually being reduced can be attributed to the prominent amount of carbon formed at this stage of reduction, and thus CO is generated by the reaction of the formed carbon and CO_2 (reverse Boudouard reaction). Moreover, high CH_4 conversion cannot be sustained in the fixed bed, when over 85% of the oxygen carrier is converted. From Fig. 9, the CH_4 conversion is 100% until 3–4 min, and after that period, the unreacted CH_4 further negatively affects the CO_2 selectivity. On the contrary, in the fluidized bed reactor, the CO_2 selectivity increases to almost 1 at a slower rate (because of the initial CH_4 slip in the bubble phase, where CH_4 quickly bypasses the oxygen carrier through the bubbles) and slowly drops to 95% when NiO conversion reaches 80%. CO_2 selectivity in the emulsion phase is higher than in the bubble phase, which corresponds to the nearly complete CH_4 conversion and negligible carbon formation of this fluidized bed unit, especially in the emulsion phase. Table 3 shows the carbon and hydrogen selectivity when 80 mol% NiO is converted. High CO_2 and low CH_4 were observed at this stage of reduction from both reactors; while some CO exists in the fixed bed outlet and more solid carbon is formed, which contributes to relatively low CO_2 selectivity. The fluidized bed reactor achieves high CO_2 selectivity and CH_4 conversion for a greater conversion span when compared to the fixed bed. It should be noted that CH_4 slip in the fluidized bed would be a smaller issue in a bed operating at steady-state with sufficient Ni to activate CH_4 conversion reactions, as discussed by Iliuta *et al.* (2010).

Temperature and Pressure Changes

As one of the advantages of operating fluidized beds, rapid mixing of solids leads to close to isothermal conditions throughout the reactor. There is lower risk of hot spots, temperature runaway and thermal instability (Jakobsen, 2008). Figs. 10(b) and 10(c) show the distribution of temperature inside the emulsion and bubble of the fluidized bed w.r.t bed length and reduction time. A low temperature zone (ΔT = 250 °C) extends from the inlet to the mid bed height of the emulsion phase and from the inlet to the quarter bed height of the bubble phase. Reactions between gas and solids continue in the bubble phase, however rates are relatively smaller and temperature drop is lower. Furthermore, temperature is partly uniform across the axial direction, which is due to the active mixing of the solids and gases. As expected, the temperature profile of the fluidized bed is more uniform than the fixed bed, shown in Fig. 10(a). Temperature fluctuations inside the fixed bed reactor reach up to 500°C from their initial values. At the cold spots inside the bed where the bed temperature is significantly lower than the desired reactor temperature, most of the CLC

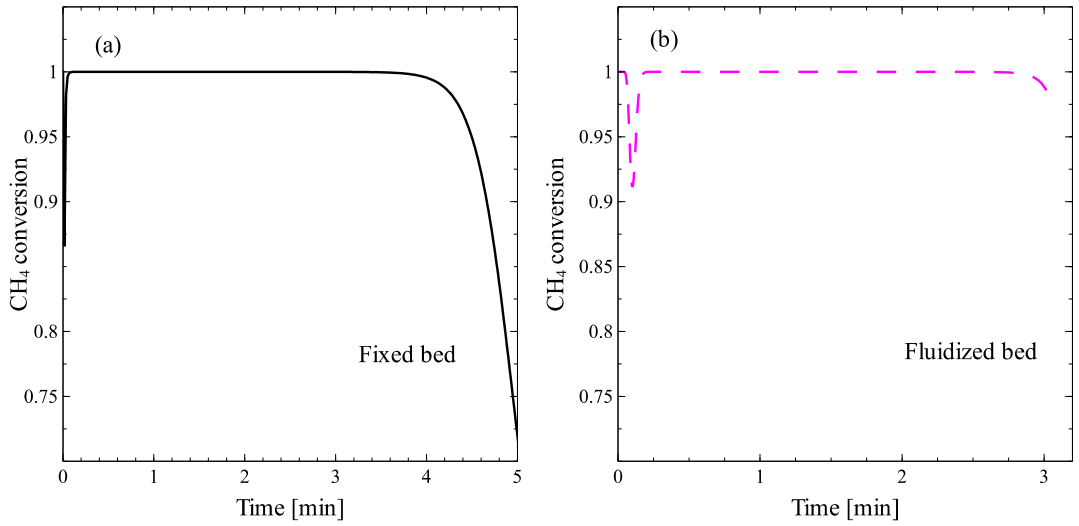

Fig. 9. Prediction of transient profiles of chemical-looping fuel conversion using Ni/NiO and CH_4 in (a) fixed bed reactor and (b) bubbling bed reactor.

Table 3. Product selectivity (carbon selectivity and hydrogen selectivity) of the fixed bed and fluidized bed units when the NiO conversion is 80 mol%.

Carbon selectivity	Fluidized bed unit	Fixed bed unit
$S_{2,CO}$	2.60	12.07
$S_{2,CO2}$	96.45	76.20
$S_{2,CH4}$	0.14	0.33
Hydrogen selectivity	**Fluidized bed unit**	**Fixed bed unit**
$S_{1,H2}$	2.42	11.45
$S_{1,H2O}$	97.55	88.21
$S_{1,CH4}$	0.03	0.34

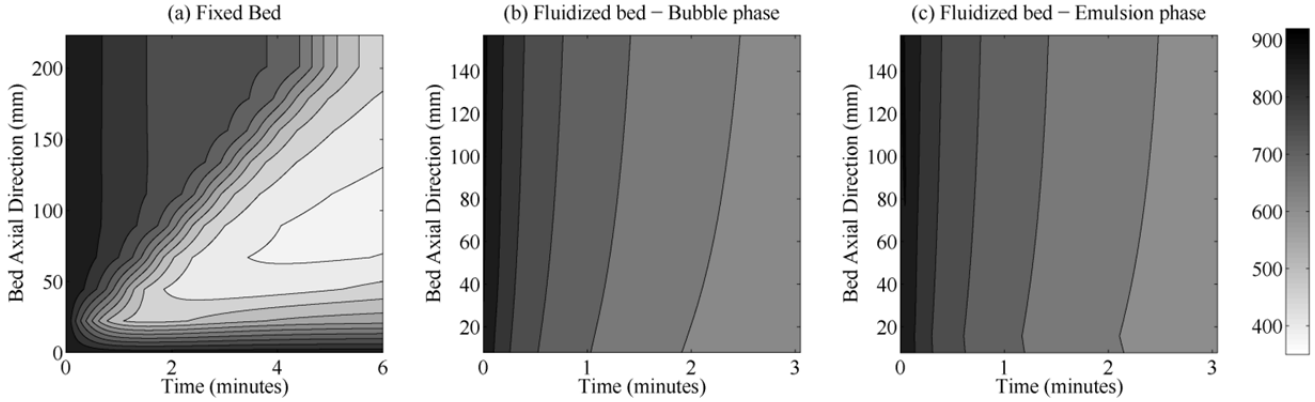

Fig. 10. Prediction of transient and spatial profiles of temperature variations (°C) in chemical-looping system using Ni/NiO and CH_4 in (a) fixed bed reactor, (b) the bubble phase and (c) emulsion phase of the bubbling bed reactor.

reactions cannot be sustained at high rate, and, therefore fuel conversion is limited.

Fig. 11 shows the pressure distribution inside the reactor. Isobaric conditions are predicted for the fluidized bed and a pressure drop of 0.6 bar is predicted for operating the fixed bed reactor. High pressure is observed at the bed entrance of the fixed bed while at the exit the pressure is set at atmospheric conditions. The impact of the high inlet pressure leads to higher overall reaction rates, and even greater temperature fluctuations. Superficial velocity is also affected by pressure effects and molar expansion, and increases along the bed height. Some transient effects observed in Fig. 11(a) are caused by changes in physical properties brought on by temperature variations.

Loading Requirement to Match Fluidized Bed Reactor

As shown in the previous sections, the performance of the fluidized bed is superior to the fixed bed in terms of

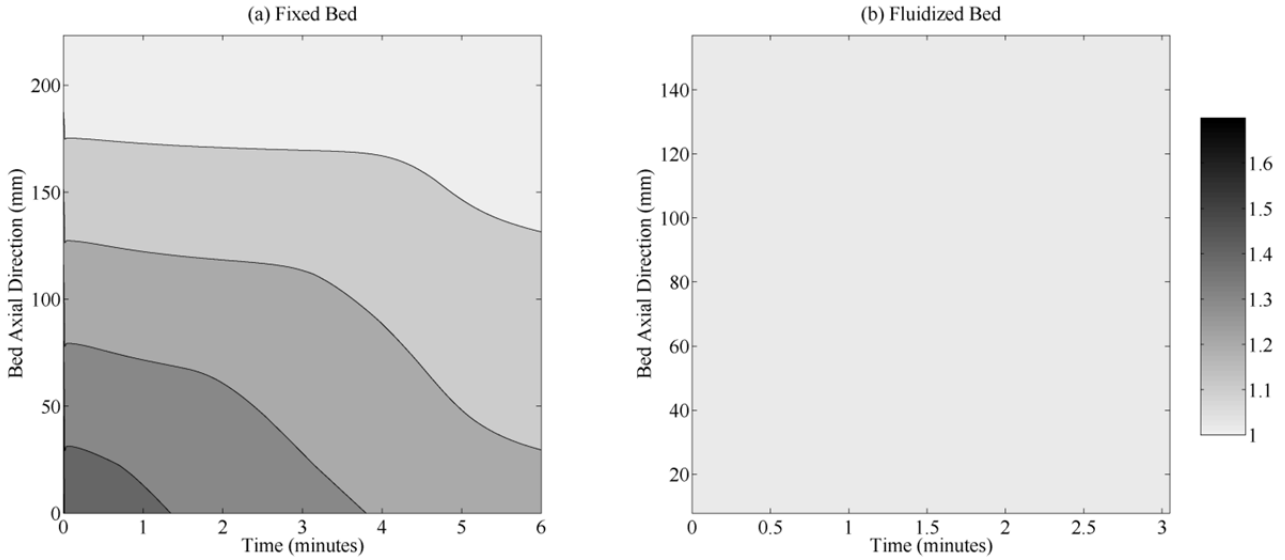

Fig. 11. Prediction of transient and spatial profiles of pressure variations (atm) in chemical-looping systems using Ni/NiO and CH_4 in (a) fixed bed reactor and (b) bubbling bed reactor.

carbon formation, CO_2 selectivity, and control of temperature and pressure. At equivalent oxygen carrier loading, the fluidized bed reactor can sustain 99% CH_4 conversion for 3 min, while the fixed bed can maintain 99% CH_4 conversion for well over 4 minutes (Fig. 9). CH_4 slip is an issue with the fluidized bed at the beginning of the reduction period where CH_4 escapes quickly through the bubble phase without conversion. In this section, different oxygen carrier loadings are explored in two scenarios: (1) in the fixed bed reactor to match the performance of the fluidized bed and (2) in the fluidized bed reactor to match the performance of the fixed bed. All other parameters, i.e., flow rate and reactor diameter, are kept constant. In the first case, by decreasing the oxygen loading of the fixed bed, the bed height is shortened and capacity of the bed is reduced. Fig. 12 shows that with decreased loading, the time to maintain 99% CH_4 conversion is shortened. About 28% less oxygen carrier loading is required to operate the fixed bed reactor in order to achieve the same time span for 99% CH_4 fuel conversion in the fluidized bed.

The scale-up of the fluidized bed reactor is also a topic of interest. The increase in time span to sustain 99% CH_4 conversion with increasing oxygen carrier loading is shown in Fig. 12. To maintain the same performance as the fixed bed reactor utilizing 2.5 kg of loading, 3.75 kg of oxygen carrier loading is required for the fluidized bed. Lower loading requirement for the fixed bed can be attributed to the higher rates of catalytic reactions which are favored to occur in the static bed. In addition to the oxygen carrier reduction reactions, reforming reactions further promote the fuel conversion. More partial combustion products (H_2, CO) are produced in the fixed bed, which was illustrated in the CO_2 selectivity comparison. Because of the effective heat and mass transfer rates between gas and solids in the fluidized bed, lower carbon formation, and better selectivity to CO_2, large-scale implementation of CLC in fluidized bed reactors is the more reasonable choice.

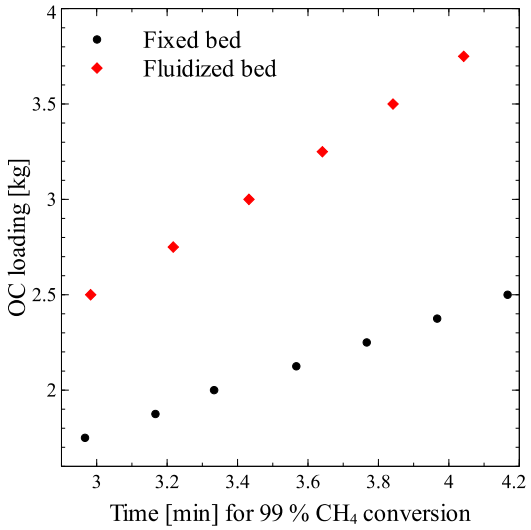

Fig. 12. Oxygen carrier required and time of maintaining 99% CH_4 conversion in chemical-looping systems using Ni/NiO and CH_4 in fixed bed reactor and bubbling bed reactor.

Cost savings can be obtained in implementing CLC in fluidized beds because of the benefits discussed in the previous paragraph. However, in a continuous fluidized bed unit, the attrition caused by the aggressive mixing and transport of solids reduces the lifetime of the oxygen carrier. Therefore, an economic analysis, including the costs of reactor set up, cost of oxygen carrier addition and environmental concerns for their disposal should be considered. The cost of the oxygen carrier is basically the main added cost of the CLC fluidized bed technology (Abad *et al.*, 2007). Attrition caused by mechanical and chemical stress poses an extra cost burden for compensating the lost material (fines). Moreover, when toxic materials are used, as in this study Ni-based oxygen carrier, the cost of fines separation and collection has to be considered.

Therefore, it is of interest to characterize the attrition behavior of oxygen carriers in fluidized bed CLC Reducers (Gayán *et al.*, 2011). As discussed in the Introduction, several experimental studies and attrition models have been carried out to investigate the long term attrition behaviors of oxygen carriers. Although modeling the attrition in fluidized bed is outside the scope of this work, it is clearly shown that all other operating aspects would favor fluidized beds in large-scale CLC implementation. Overall, low-cost, non-toxic oxygen carriers would be preferable, or technologies that limit attrition, such as simulated moving bed reactors or reverse flow fixed bed reactors.

CONCLUSIONS

This study is focused on a thorough comparison between fixed bed and fluidized bed reactors with respect to reactor efficiency and oxygen carrier utilization. Validated transient non-ideal reactor models, developed for fixed and bubbling fluidized beds were used to predict CLC system performance for Ni-based oxygen carrier using CH_4 as fuel. With the same amount of oxygen carrier, loading and CH_4 flow rate for both setups, the dimensions of the fixed bed reactor were selected from a scale-up analysis of a micro-reactor to match the capacity of a fluidized bed reactor. Most of the CLC Reducer performance indices of industrial interest, such as CO_2 selectivity, fuel conversion, oxygen carrier conversion, carbon formation, temperature and pressure profiles, were discussed. Compared to a fixed bed Reducer, a fluidized bed is more appropriate for large-scale implementation of the CLC process because of its uniform temperature and pressure distribution, high CO_2 selectivity (> 95%), negligible carbon formation (< 2 mol% C basis), and high fuel conversion (> 90%) over longer reduction periods. However, the main drawback of implementing CLC in a continuous fluidized bed reactor is the added cost for compensating the lost fines, caused by attrition of the oxygen carrier in the relatively aggressive fluidized bed conditions. This work delivers a performance analysis of the different types of bench-scale CLC Reducers and scale-up of the fluidized bed reactor is underway.

ACKNOWLEDGEMENTS

This material is based upon work supported by the National Science Foundation under Grant No. 1054718.

NOMENCLATURE

A Cross-sectional area of the reactor tube [m^2]
Ar Archimedes number, $Ar = d_P^3 \rho_g (\rho_P - \rho_g) g / \mu_g^2$
C_i Bulk concentration of gaseous reactant i [$kmol/m^3$]
C_{pf} Heat capacity of the gas mixture of the fluid phase [J/mol-k]
C_T Total gas concentration in fluid phase [mol/m^3]
D_R Reactor diameter [m]
$D_{ax,i}$ Axial dispersion coefficient of species i [m^2/s]
d_P Particle diameter [m]
d_P^* Dimensionless particle diameter
$D_{rad,i}$ Radial dispersion coefficient of species i [m^2/s]
f Fraction of gas or solid in the bubble or emulsion phase
F_i Molar flow rate of gas species i [mol/s]
F_T Total molar flow rate of gas species [mol/s]
G_m Rate of heat transfer cross-flow between two phases [W/m], $G_b = -G_e$
H Bed height [m]
$H_{k,m}$ Heat transfer between bubble and emulsion or emulsion and bubble [W/m^3-K]
$K_{i,m}$ Gas exchange coefficient between bubble-emulsion or emulsion-bubble [s^{-1}]
$K_{j,m}$ Solid exchange coefficient between wake-emulsion or emulsion-wake [s^{-1}]
$K_{s,j,m}$ Rate of solid phase cross-flow between two phases [mol/m-s], $K_{s,j,b} = -K_{s,j,e}$
$K_{g,j,m}$ Rate of gas phase cross-flow between two phases [mol/m-s], $K_{g,j,b} = -K_{g,j,e}$
M_i Molecular weight [kg/kmol]
r Reactor radial element
R Reaction rate [mol/g_{Ni}-s]
Re Reynolds number, $Re = \rho_g u d_P / \mu_g$
$S_{1,j}$ H_2 selectivity
$S_{2,j}$ Carbon selectivity
t Time element [s]
T Temperature [°C]
u_m Velocity of phase m [m/s]
V Volume element [m^3]
X NiO conversion
z Length element

Greek letters

ε_{bed} Porosity of the bed
ε_F Freeboard bed voidage
ΔH_n Heat of reaction n [J/mol]
ρ_P Particle density [kg/m^3]
λ_{ax} Axial heat dispersion coefficient [W/m-K]
λ_{rad} Radial heat dispersion coefficient [W/m-K]
R_k Reaction term, $\rho_P \sum R_{j,m}$ (when $k = i$), or $M_j \sum R_{j,m}$ (when $k = j$)

Subscripts

f fluid
F freeboard
g gas
i gas species (CH_4, H_2, H_2O, CO, CO_2, Ar, N_2)
j solid species (Ni, NiO, C, inert support)
k gas or solid species
m bubbles or emulsion
n reaction
P particle
q i (when k is gas) or j (when k is solid)

APPENDIX

Two-dimensional Homogeneous Model Design Equations (Han et al., 2013)

$$\varepsilon_{bed}\frac{\partial C_i}{\partial t}+\frac{\partial F_i}{\partial V}=\varepsilon_{bed}\frac{\partial}{\partial z}\left(D_{ax,i}\frac{\partial C_i}{\partial z}\right)+\frac{\varepsilon_{bed}}{r}\left(rD_{rad,i}\frac{\partial C_i}{\partial r}\right)+\rho_P\sum R_i \quad (1)$$

$$\varepsilon_{bed}Cp_fC_T\frac{\partial T}{\partial t}+Cp_fF_T\frac{\partial T}{\partial V}=\varepsilon_{bed}\frac{\partial}{\partial z}\left(\lambda_{ax}\frac{\partial T}{\partial z}\right)+\frac{\varepsilon_{bed}}{r}\frac{\partial}{\partial r}\left(r\lambda_{rad}\frac{\partial T}{\partial r}\right)+\rho_P\sum(-\Delta H_n)(R_n) \quad (2)$$

One-dimensional Three Phase Dynamic Model Design Equations (Zhou et al., 2014)

Mass balance (Gas or solid in the bubble/wake and emulsion phases):

$$f_{k,m}\frac{\partial C_{q,m}}{\partial t}+\frac{\partial(u_mf_{k,m}C_{q,m})}{\partial z}=K_{q,m}\Delta C_if_{k,m}+\frac{K_{k,q,m}}{A}+f_{s,m}R_k \quad (3)$$

Energy balance (Bubble and emulsion phases):

$$\sum(f_{k,m}Cp_{k,m}C_{T,k,m})\frac{\partial T_m}{\partial t}+\sum(f_{k,m}Cp_{k,m}C_{T,k,m}u_m)\frac{\partial T_m}{\partial z}=H_{k,m}\Delta T_mf_{k,m}+\frac{G_m}{A}+f_{s,m}\rho_P\sum(-\Delta H_{n,m})(-R_{n,m}) \quad (4)$$

Freeboard region:

$$\varepsilon_F\frac{\partial C_{i,f}}{\partial t}+u_{g,F}\frac{\partial C_{i,F}}{\partial z}=(1-\varepsilon_F)R_{i,F}\rho_p \quad (5)$$

$$(1-\varepsilon_F)\frac{\partial C_{j,F}}{\partial t}+u_{s,F}\frac{\partial C_{j,F}}{\partial z}=(1-\varepsilon_F)R_{j,F}M_j \quad (6)$$

$$\sum(f_{k,F}Cp_{k,F}C_{T,k,F})\frac{\partial T_F}{\partial t}+\sum Cp_{k,F}C_{T,k,F}u_{k,F}\frac{\partial T_F}{\partial z}=(1-\varepsilon_F)\rho_P\sum\left(-\Delta H_{n,F}\right)\left(-R_{n,F}\right) \quad (7)$$

REFERENCES

Abad, A., Adánez, J., García-Labiano, F., De Diego, L.F., Gayán, P. and Celaya, J. (2007). Mapping of the Range of Operational Conditions for Cu-, Fe-, and Ni-Based Oxygen Carriers in Chemical-Looping Combustion. *Chem. Eng. Sci.* 62: 533–549.

Adánez, J., Gayán, P. and Celaya, J. (2006). Chemical Looping Combustion in a 10 kW_{th} Prototype Using a CuO/Al_2O_3 Oxygen Carrier: Effect of Operating Conditions on Methane Combustion. *Ind. Eng. Chem. Res.* 45: 6075–6080.

Adánez, J., Dueso, C., De Diego, L.F., García-Labiano, F., Gayán, P. and Abad, A. (2009). Effect of Fuel Gas Composition in Chemical-Looping Combustion with Ni-Based Oxygen Carriers. 2. Fate of Light Hydrocarbons. *Ind. Eng. Chem. Res.* 48: 2509–2518.

Adánez, J., Abad, A., García-Labiano, F., Gayán, P. and De Diego, L.F. (2012). Progress in Chemical-Looping Combustion and Reforming Technologies. *Prog. Energy Combust. Sci.* 38: 215–282.

ASTM (1995). ASTM D5757-95: Standard Test Method for Determination of Attrition and Abrasion of Powdered Catalysts by Air Jets.

Baek, J., Ryu, C., Kim, J., Ryu, J., Lee, J., Eom, T. and Yi, J. (2010). Spray-Dried NiO Oxygen Carrier with Highly Attrition Resistance, Proc. 1st International Conference on Chemical Looping, Lyon, France.

Baek, J.I., Ryu, J., Lee, J.B., Eom, T.H., Kim, K.S., Yang, S.R. and Ryu, C.K. (2011). Highly Attrition Resistant Oxygen Carrier for Chemical Looping Combustion. *Energy Procedia* 4: 349–355.

Bi, H. and Grace, J. (1995). Flow Regime Diagrams for Gas-Solid Fluidization and Upward Transport. *Int. J. Multiphase Flow* 21: 1229–1236.

Chandel, M.K., Hoteit, A. and Delebarre, A. (2009). Experimental Investigation of Some Metal Oxides for Chemical Looping Combustion in a Fluidized Bed Reactor. *Fuel* 88: 898–908.

Corbella, B.M., de Diego, L.F., García-Labiano, F., Adánez, J. and Palaciost, J.M. (2005). Characterization Study and Five-cycle Tests in a Fixed Bed Reactor of Titania-supported Nickel Oxide as Oxygen Carriers for the Chemical-looping Combustion of Methane. *Environ. Sci. Technol.* 39: 5796–5803.

García-Labiano, F., de Diego, L.F., Adánez, J. and Abad, A., Gayán, P. (2005). Temperature Variations in the Oxygen Carrier Particles during Their Reduction and Oxidation in a Chemical-looping Combustion System. *Chem. Eng. Sci.* 60: 851–862.

Gayán, P., Forero, C.R., Abad, A., Diego, L.F., García-labiano, F. and Adánez, J. (2011). Effect of Support on the Behavior of Cu-Based Oxygen Carriers during Long-Term CLC Operation at Temperatures above 1073 K. *Energy Fuels* 25: 1316–1326.

Håkonsen, S.F. and Blom, R. (2011). Chemical Looping Combustion in a Rotating Bed Reactor--Finding Optimal Process Conditions for Prototype Reactor. *Environ. Sci. Technol.* 45: 9619–26.

Han, L., Zhou, Z. and Bollas, G.M. (2013). Heterogeneous Modeling of Chemical-Looping Combustion. Part 1: Reactor Model. *Chem. Eng. Sci.* 104: 233–249.

IEA (2011). IEA. International Energy Agency: CO_2 Emission from Fuel Combustion Highlights.

Iliuta, I., Tahoces, R., Patience, G.S., Rifflart, S. and Luck, F. (2010). Chemical-Looping Combustion Process: Kinetics and Mathematical Modeling. *AIChE J.* 56: 1063–1079.

Jakobsen, H.A. (2008). *Chemical Reactor Modeling - Multiphase Reactive Flows*. Springer Berlin Heidelberg, Trondheim, Norway.

Jerndal, E., Mattisson, T. and Lyngfelt, A. (2006). Thermal Analysis of Chemical-Looping Combustion. *Chem. Eng. Res. Des.* 84: 795–806.

Jin, H. and Ishida, M. (2002). Reactivity Study on Natural-Gas-Fueled Chemical-Looping Combustion by a Fixed Bed Reactor. *Ind. Eng. Chem. Res.* 41: 4004–4007.

Kim, W., Yun, C., Jung, K.T., Park, S. and Kim, S.H. (2012). Computer-Aided Scale-up of a Packed Bed Tubular Reactor. *Comput. Chem. Eng.* 39: 96–104.

Kolbitsch, P., Bolhàr-Nordenkampf, J., Pröll, T. and Hofbauer, H. (2009). Comparison of Two Ni-Based Oxygen Carriers for Chemical Looping Combustion of Natural Gas in 140 kW Continuous Looping Operation. *Ind. Eng. Chem. Res.* 48: 5542–5547.

Kramp, M., Thon, A., Hartge, E.U., Heinrich, S. and Werther, J. (2011) The Role of Attrition and Solids Recovery in a Chemical Looping Combustion Process. *Oil Gas Sci. Technol.* 66: 277–290.

Kunii, D. and Levenspiel, O. (1968a). Bubbling Bed Model for Kinetic Processes in Fluidized Beds: Gas-Solid Mass and Heat Transfer and Catalytic Reactions. *Ind. Eng. Chem. Process Des. Dev.* 7: 481–492.

Kunii, D. and Levenspiel, O. (1968b). Bubbling Bed Model: Model for the Flow of Gas Through a Fluidized Bed. *Ind. Eng. Chem. Fundam.* 7: 446–452.

Kunii, D. and Levenspiel, O. (1997). Circulating Fluidized Bed Reactors. *Chem. Eng. Sci.* 52: 2471–2482.

Lyngfelt, A., Leckner, B. and Mattisson, T. (2001). A Fluidized Bed Combustion Process with Inherent CO_2 Separation: Application of Chemical-Looping Combustion. *Chem. Eng. Sci.* 56: 3101–3113.

Lyngfelt, A. and Thunman, H. (2005). Construction and 100 h of Operational Experience of a 10-kW Chemical-Looping Combustor, In *The CO_2 Capture and Storage Project (CCP) for Carbon Dioxide Storage in Deep Geologic Formations For Climate Change Mitigation*, Thomas, D. (Ed.), Elsevier Science, London.

Mattisson, T., Johansson, M. and Lyngfelt, A. (2004). Multicycle Reduction and Oxidation of Different Types of Iron Oxide Particles Application to Chemical-Looping Combustion. *Energy Fuels* 18: 628–637.

Mattisson, T., Johansson, M. and Lyngfelt, A. (2006). The Use of NiO as an Oxygen Carrier in Chemical-Looping Combustion. *Fuel* 85: 736–747.

Mattisson, T., Lyngfelt, A. and Leion, H. (2009). Chemical-Looping with Oxygen Uncoupling for Combustion of Solid Fuels. *Int. J. Greenhouse Gas Control* 3: 11–19.

Nauman, E.B. (2008). *Chemical Reactor Design, Optimization, and Scaleup*, Wiley-AIChE.

Noorman, S., Van Sint Annaland, M. and Kuipers, H. (2007). Packed Bed Reactor Technology for Chemical-Looping Combustion. *Ind. Eng. Chem. Res.* 46: 4212–4220.

Olazar, M., San José, M.J., Alvarez, S., Morales, A. and Bilbao, J. (2004). Design of Conical Spouted Beds for the Handling of Low-Density Solids. *Ind. Eng. Chem. Res.* 43: 655–661.

Olazar, M., López, G., Altzibar, H., Aguado, R. and Bilbao, J. (2009). Minimum Spouting Velocity under Vacuum and High Temperature in Conical Spouted Beds. *Can. J. Chem. Eng.* 87: 541–546.

Pröll, T., Kolbitsch, P., Bolhar-Nordenkampf, J. and Hofbauer, H. (2009). A Novel Dual Circulating Fluidized Bed System for Chemical Looping Processes. *AIChE J.* 55: 3255–3266.

Rhodes, M. (2008). *Introduction to Particle Technology*, John Wiley and Sons.

Rifflart, S., Hoteit, A., Yazdanpanah, M.M., Pelletant, W. and Surla, K. (2011). Construction and Operation of a 10 kW CLC Unit with Circulation Configuration Enabling Independent Solid Flow Control. *Energy Procedia* 4: 333–340.

Rubin, E.S., Mantripragada, H., Marks, A., Versteeg, P. and Kitchin, J. (2012). The Outlook for Improved Carbon Capture Technology. *Prog. Energy Combust. Sci.* 38: 630–671.

Rydén, M., Lyngfelt, A., Mattisson, T., Chen, D., Holmen, A. and Bjørgum, E. (2008). Novel Oxygen-carrier Materials for Chemical-looping Combustion and Chemical-looping Reforming; $La_xSr_{1-x}Fe_yCo_{1-y}O_{1-3-\delta}$ Perovskites and Mixed-metal Oxides of NiO, Fe_2O_3 and Mn_3O_4. *Int. J. Greenhouse Gas Control* 2: 21–36.

Ryu, H., Bae, D. and Jin, G. (2003). Effect of Temperature on Reduction Reactivity of Oxygen Carrier Particles in a Fixed Bed Chemical-looping Combustor. *Korean J. Chem. Eng.* 20: 960–966.

Ryu, H., Jin, G. and Yi, C. (2004). Demonstration of Inherent CO_2 Separation and No NO_x Emission in a 50 kW Chemical-Looping Combustor: Continuous Reduction and Oxidation Experiment, Proceedings of the 7th International Conference on Greenhouse Gas Control Technologies, Vancouver.

Ryu, H., Shun, D., Bae, D. and Park, M. (2009). Syngas Combustion Characteristics of Four Oxygen Carrier Particles for Chemical-looping Combustion in a Batch Fluidized Bed Reactor. *Korean J. Chem. Eng.* 26: 523–527.

Sedor, K.E., Hossain, M.M. and de Lasa, H.I. (2008). Reactivity and Stability of Ni/Al_2O_3 Oxygen Carrier for Chemical-Looping Combustion (CLC). *Chem. Eng. Sci.* 63: 2994–3007.

Solomon, S., Qin, D., Manning, M., Marquis, M., Averyt, K., Tignor, M.M.B., Miller, H.L. and Chen, Z. (2007). IPCC, 2007: Summary for Policymakers, Climate Change 2007: The Physical Science Basis. Contribution of Working Group I to the Fourth Assessment Report of the Intergovernmental Panel on Climate Change. Cambridge University Press, Cambridge, UK and NY, USA.

Solunke, R.D. and Veser, G. (2010). Hydrogen Production via Chemical Looping Steam Reforming in a Periodically Operated Fixed Bed Reactor. *Ind. Eng. Chem. Res.* 49: 11037–11044.

Sridhar, D., Tong, A., Kim, H., Zeng, L., Li, F. and Fan, L. (2012). Syngas Chemical Looping Process: Design and Construction of a 25 kW_{th} Subpilot Unit. *Energy Fuels* 26: 2292–2302.

Toftegaard, M.B., Brix, J., Jensen, P.A., Glarborg, P. and Jensen, A.D. (2010). Oxy-Fuel Combustion of Solid Fuels. *Prog. Energy Combust. Sci.* 36: 581–625.

Wang, S., Wang, G., Jiang, F., Luo, M. and Li, H. (2010). Chemical Looping Combustion of Coke Oven Gas by Using Fe_2O_3/CuO with $MgAl_2O_4$ as Oxygen Carrier. *Energy Environ. Sci.* 3: 1353.

Yang, W.C. (2003). *Handbook of Fluidization and Fluid-*

Particle Systems, Marcel Dekker, Inc., New York.
Zhou, Z., Han, L. and Bollas, G.M. (2013). Model-based Analysis of Bench-Scale Fixed Bed Units for Chemical-Looping Combustion. *Chem. Eng. J.* 233: 331–348.
Zhou, Z., Han, L. and Bollas, G.M. (2014). Modeling Chemical-Looping Combustion in Bubbling Fluidized Bed Reactors. In Preparation.

Received for review, June 17, 2013
Accepted, November 2, 2013